AGU PUBLICATIONS

Geophysical Research Letters

RESEARCH LETTER
10.1002/2017GL076544

Key Points:
- The CO_2 north of 60°N varies with an amplitude of ±0.6 ppm over the MJO cycle
- The spatial pattern of the MJO-related Arctic CO_2 anomalies resembles that of the isentropic potential vorticity anomalies at 475 K
- The reported CO_2 variability would help improve chemistry transport modeling

Supporting Information:
- Supporting Information S1

Correspondence to:
K.-F. Li,
king-fai.li@ucr.edu

Citation:
Li, K.-F. (2018). An intraseasonal variability in CO_2 over the Arctic induced by the Madden-Julian Oscillation. *Geophysical Research Letters, 45*. https://doi.org/10.1002/2017GL076544

Received 24 NOV 2017
Accepted 9 JAN 2018
Accepted article online 18 JAN 2018

An Intraseasonal Variability in CO_2 Over the Arctic Induced by the Madden-Julian Oscillation

King-Fai Li[1,2]

[1]Department of Applied Mathematics, University of Washington, Seattle, WA, USA, [2]Department of Environmental Sciences, University of California, Riverside, CA, USA

Abstract Variability of atmospheric CO_2 must be well understood for us to better characterize the anthropogenic CO_2 release from the surface. A previous study revealed the influence of the Madden-Julian Oscillation (MJO) to tropical midtropospheric CO_2 via convection. In this work, the observations by NASA's Atmospheric Infrared Sounder are used to further examine the MJO impact on the CO_2 concentration over the Arctic. A composite analysis shows that the CO_2 north of 60°N varies with a peak-to-peak amplitude of 1.2 ± 0.2 ppm over the MJO cycle. An empirical correlation analysis is applied to examine possible effects of retrieval bias and dynamics on the MJO-related CO_2 anomalies. It is shown that the spatial pattern of the MJO-related Arctic CO_2 anomalies closely resembles that of the isentropic potential vorticity anomalies at 475 K.

1. Introduction

Carbon dioxide (CO_2) is the most important anthropogenic greenhouse gas in Earth's atmosphere. As of 2016, CO_2 concentration in the atmosphere has passed the historical 400 parts per million by volume (ppm) (World Meteorological Organization, 2016). Each year, ~8.9 pentagram of carbon equivalent per year (Pg C/yr) of CO_2 from fossil fuel burning and net land use change is released to the atmosphere, of which 2.6 Pg C/yr and 2.3 Pg C/yr are taken up by the terrestrial biosphere and the ocean, respectively, and the remaining 4.0 Pg C/yr accumulates in the atmosphere (Ciais et al., 2013). These budget estimates are based on official figures and ground-based measurements of CO_2 and are subject to an uncertainty of ~1 Pg C/yr (at the 10% significance level) (see Table 6.1 of Ciais et al., 2013). If we are to improve these estimates to better than 1 Pg C/yr, global CO_2 column measurements are required to have a precision less than 2 ppm (Rayner & O'Brien, 2001). At such precision, some natural variability of CO_2 (e.g., induced by El Niño–Southern Oscillation) become discernible and, if not treated properly, would interfere with the anthropogenic budget estimations (e.g., Gruber et al., 1999; Hashimoto et al., 2004; Keppel-Aleks et al., 2012; Le Quéré et al., 2003). It then follows that the natural variability of atmospheric CO_2 must also be well understood in order to better characterize the influence of anthropogenic CO_2 to climate.

Continuous measurements from space (Buchwitz et al., 2005; Chahine et al., 2008; Crevoisier et al., 2009; Eldering et al., 2017; Kuze et al., 2009; Nassar et al., 2011) and ground (Nevison et al., 2008; Newman et al., 2016; Wong et al., 2015; Wunch et al., 2011) have been devoted to monitoring atmospheric CO_2 variability on daily to monthly basis. With midtropospheric CO_2 observations from NASA's spaceborne Atmospheric Infrared Sounder (AIRS) becoming available in the last decade (Chahine et al., 2008), several short-term (intraseasonal to interannual) natural variability have been unveiled, including the tropical intraseasonal variability (with peak-to-peak amplitude ~1.5 ppm) related to the Madden-Julian oscillation (MJO) (Li et al., 2010), the semiannual variability (~3 ppm) (Jiang et al., 2012), the biennial variability (~1.0 ppm) related to Asian monsoons (Wang et al., 2011), interannual variability (2–3 ppm) related to the El Niño–Southern Oscillation (Jiang et al., 2010), and polar variability related to the Arctic oscillation and stratospheric sudden warming (Jiang et al., 2010, 2013).

Convection brings CO_2-rich air from the lower troposphere to the midtroposphere, and AIRS observes this increase in the midtropospheric CO_2 (Chahine et al., 2008). However, individual convection events are highly variable and are of kilometer scales that are much smaller than the AIRS footprints (~13.5 km). Given that tropospheric CO_2 is well mixed and that the difference between the surface and the midtropospheric CO_2 abundance is small (~1.5 ppm), identifying individual convection events in an AIRS footprint is therefore extremely challenging. In contrast, by averaging over a dozen of MJO events during the measurement

period, the impact of large-scale convection on the CO_2 distribution over the MJO cycle can be identified with statistical significance (Li et al., 2010). The discovery of the MJO signals in AIRS CO_2 observations implies that midtropospheric CO_2 can be organized by short-term processes that are relevant to weather prediction time scales. Here Li et al.'s (2010) analysis will be extended to polar latitudes.

2. Data and Method

The AIRS daily CO_2 observations since 2002 are currently the longest global CO_2 data available (Chahine et al., 2008). The AIRS instrument measures spectral radiance between 650 and 2,600 cm^{-1} with a 13.5 km nadir field of view (Aumann et al., 2003).The mixing ratios of CO_2 have been retrieved from the spectral channels between 690 and 725 cm^{-1} using vanishing partial derivatives (Chahine et al., 2005) for clear-sky footprints. At least three valid AIRS Level 2 retrievals in a 2×2 grouping of adjacent retrievals under clear-sky conditions are required to create a Level 3 daily average at a grid point. Before 2012, the AIRS retrievals are incorporated with the cloud information from a companion instrument, advanced microwave sounding unit (AMSU), at a coarser spatial resolution of 45 km in the nadir (Susskind et al., 2003). Because of the degradation of AMSU, the AIRS retrievals after 2012 rely only on infrared measurements. For better cloud-cleared measurements, we shall only use AIRS/AMSU coretrievals of CO_2 in this study. The AIRS version 5 CO_2 Level 3 product has been gridded onto 2.5° longitude × 2.0° latitude boxes. Validation against in situ aircraft and ground-based measurements demonstrates an accuracy of 2 ppmv for individual retrievals of AIRS CO_2 between latitudes 30°S and 80°N.

The MJO is the dominant form of tropical intraseasonal variability (Madden & Julian, 1971, 1972). In brief, a typical MJO cycle is characterized by enhanced convective activity over the equatorial Indian Ocean, followed by a slow eastward propagation (~5 m s^{-1}), passing the Maritime Continent and moving into the central Pacific. The propagation ends with a weakening of the convective disturbances when reaching the eastern Pacific. The whole cycle lasts 40–60 days (Hendon & Salby, 1994). The life cycle of the MJO is characterized by the Real-time Multivariate MJO index (Wheeler & Hendon, 2004), where the MJO is divided into eight phases and each phase corresponds to 5–7 days. Phase 1 is characterized by an enhanced tropical convection over the western Indian Ocean, which propagates eastward at a speed of ~5 m s^{-1} in the subsequent phases until it reaches the central Pacific and weakens in Phase 8. A given date is assigned with an MJO phase according to the MJO index. To extract the MJO signal in CO_2, the CO_2 time series at each AIRS grid point is deseasonalized, followed by a band-pass filtering to capture variability between 15 and 90 days. The CO_2 anomalies at each grid point in each MJO phase are averaged.

3. Results

The MJO-related propagation of the CO_2 anomalies over the tropical region has been discussed in Li et al. (2010). Figure 1 focuses on the MJO composites of the CO_2 anomalies in the Northern Hemisphere. For visualization, the eight MJO phases are further combined to four phases: Phases 8 and 1 as Phase 8 + 1, Phases 2 and 3 as Phase 2 + 3, Phases 4 and 5 as Phase 4 + 5, and Phases 6 and 7 as Phase 6 + 7. The eastward propagation of the MJO disturbance is indicated by the rainfall anomalies (black solid/dashed lines), obtained from the Tropical Rainfall Measuring Mission 3B42 product (Huffman et al., 2007). Overlaid in Figure 1 are the anomalies of the isentropic potential vorticity at the 475 K isentrope (potential vorticity $(PV)_{475K}$), which will be discussed in section 4.

Phase 8 + 1 is characterized by an MJO disturbance over the western Indian Ocean (indicated by the enhanced rainfall at the "R+" sign in Figure 1). During this phase, the Arctic CO_2 is reduced by 0.6 ppm over most of the Arctic region (north of 45°N) except over the Bering Sea, where the Arctic CO_2 is enhanced by 0.6 ppm. In Phase 2 + 3, the enhanced rainfall has moved to the Maritime Continents. During this phase, the spatial distribution of the Arctic CO_2 anomalies is less well defined compared with that in the previous phase. There are small-scale enhancements over Siberia, Alaska, and the North Atlantic in the Arctic region. There are also small-scale reductions over Greenland, the eastern Europe, and the northeastern China. In Phase 4 + 5, the enhanced rainfall has moved to the western Pacific. During this phase, the spatial distribution of the Arctic CO_2 anomalies is nearly opposite to that during Phase 8 + 1: There are strong reductions in the Arctic CO_2 over the Bering Sea and the Siberia and enhancements over North America, North Atlantic, and

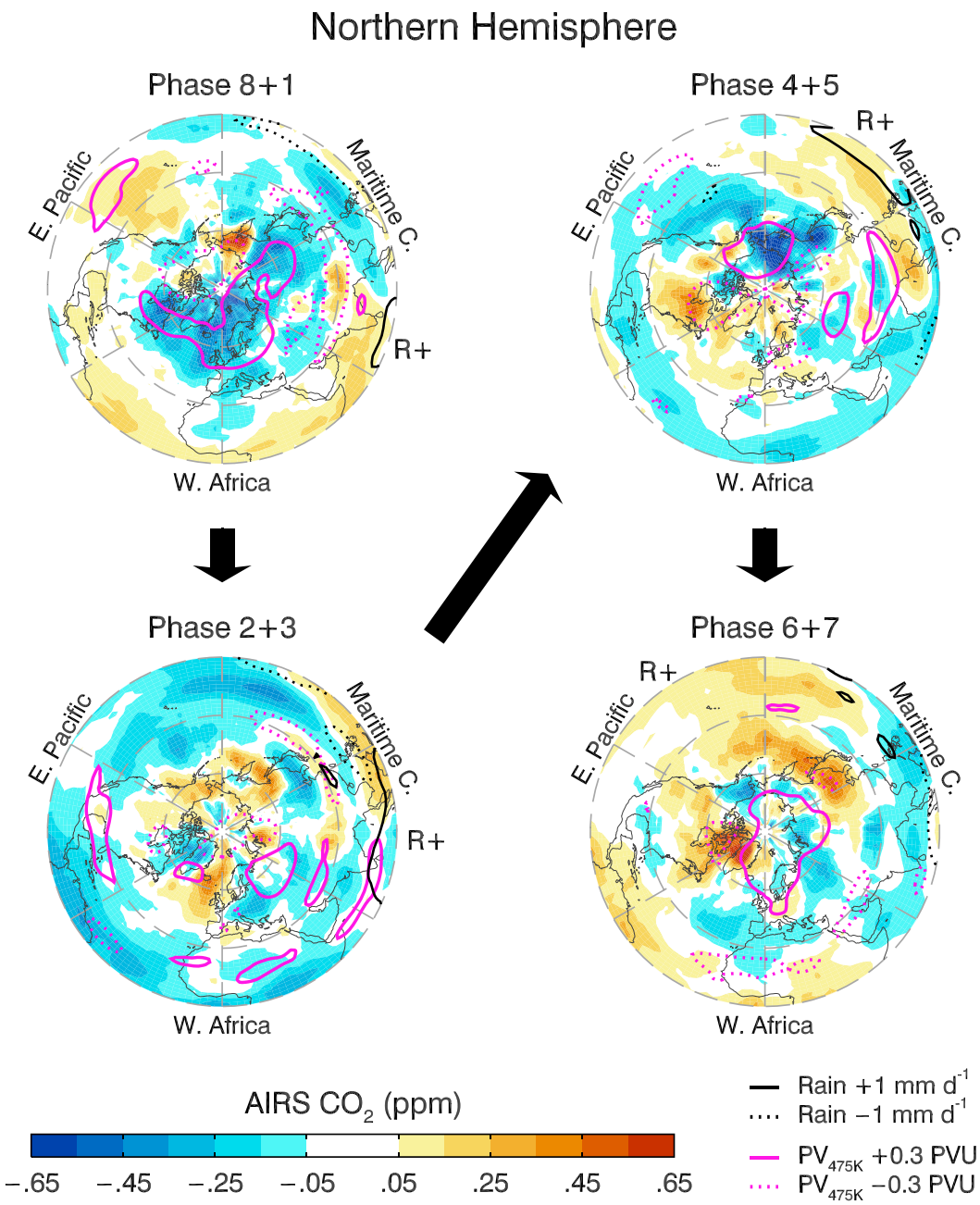

Figure 1. MJO-related AIRS CO_2 anomalies. The propagation of the MJO is indicated by the rainfall anomalies (black contour lines) and by the R+ sign that traces the movement of the positive rainfall anomalies. For visualization, a 10° longitude × 8° latitude running average is applied to CO_2 anomalies to remove high-wave number spatial fluctuations. The pink contour lines show the anomalies of the isentropic potential vorticity at the 475 K isentrope (PV_{475K}).

most of Europe. Lastly, in Phase 6 + 7, the MJO disturbance has reached the western Pacific and is dying out. During this phase, there are reductions in the Arctic CO_2 over most of the Eurasia and Alaska, flanked by the enhancements over Greenland and northeast China. In summary, the MJO-related Arctic CO_2 variability has an amplitude of ±0.6 ppm or 1.2 ppm peak to peak.

To verify that the MJO-related CO_2 anomalies are statistically significant, Figure 2 shows the number of AIRS CO_2 soundings averaged in each MJO phase. At low latitudes, the number of soundings may be of order 200–300. In contrast, due to the persistent presence of clouds around the polar vortex, the number of soundings are of order 60–100 in each pair of MJO phases over the Arctic region. The standard errors associated with the MJO-related CO_2 anomalies over the Arctic region are of order $\sigma/\sqrt{N}$ ~ ±0.1 ppm or 0.2 ppm

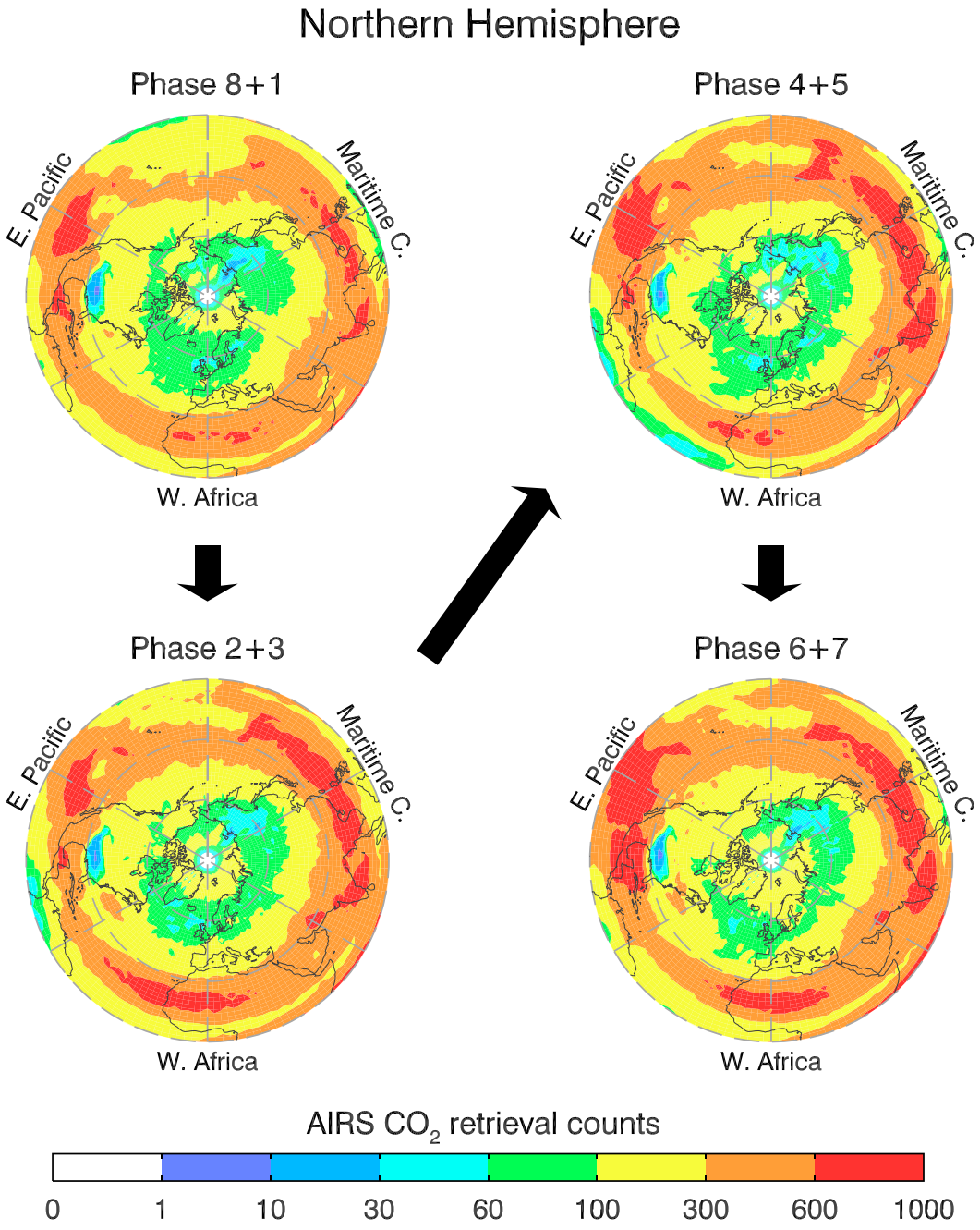

Figure 2. Number of AIRS observations being averaged in each MJO phase. The eight MJO phases originally defined by the RMM index (Wheeler & Hendon, 2004) have been simplified to four composite phases. Each panel thus represents a period of ~12 days. Only days that satisfy $RMM_1^2 + RMM_2^2 \geq 1$ are included in the composite mean calculation.

peak to peak, which is less than 20% of the MJO amplitude presented above. Thus, the spatial patterns of CO_2 anomalies shown in Figure 1 are statistically robust.

There may be a concern whether the MJO-related CO_2 anomalies are actually retrieval biases resulting from undetected clouds in the field of view. Observations over a cloudy scene may have a lower average brightness temperature than observations over a clear-sky scene due to cooler cloud top temperatures. Detecting small-scale clouds (e.g., 0.1–1 km) in the infrared is challenging because of the relatively coarse horizontal resolution provided by the infrared measurements (e.g., AIRS footprint ~13 km × 13 km). As a result, a scene with undetected high cloud might be misidentified as a "clear sky" and the corresponding

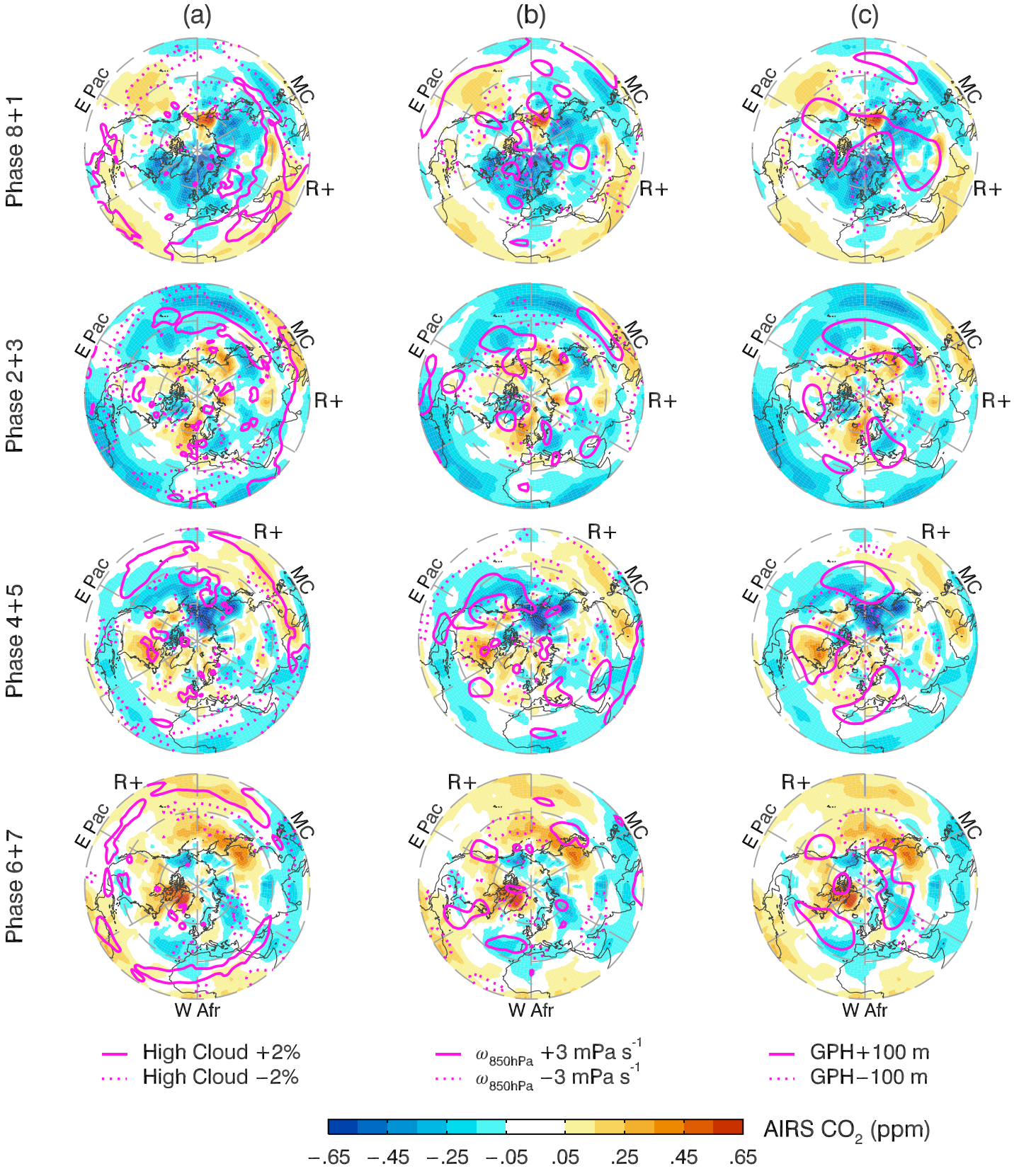

Figure 3. Correlating the MJO-related CO_2 anomalies with tropospheric variables (pink contour lines in each column): (a) high cloud fractions, (b) vertical pressure velocity at 850 hPa, and (c) geopotential height (GPH) at 500 hPa.

Table 1
The Correlation Coefficients Between the MJO-Related Potential Vorticity (PV) Anomalies and the MJO-Related CO_2 Anomalies Over Arctic (North of 45°N) at the Isentropes 350 K, 380 K, 475 K, and 530 K

	PV_{350K}	PV_{380K}	PV_{475K}	PV_{530K}
Correlation	−0.02	−0.21	−0.44	−0.32

Note. See Figure S1 in supporting information.

infrared spectrum might have a lower brightness temperature than expected. If this bias in the brightness temperature is treated as a part of the CO_2 absorption during the retrieval, the retrieved CO_2 concentrations would be overestimated. To verify whether undetected cloudy scenes might have affected the MJO-related CO_2 anomalies, Figure 3a overlays the MJO-related high cloud fraction anomalies on the MJO-related CO_2 anomalies. The high cloud fraction is obtained from European Centre for Medium-Range Weather Forecasts (ECMWF)-Interim Reanalysis. The high cloud fraction anomalies do not reveal large-scale structures, and the correlation coefficient between the high cloud fraction and CO_2 anomalies over the Arctic region is only 0.09. Therefore, the Arctic CO_2 anomalies are unlikely to be caused by undetected high cloud.

Li et al. (2010) showed that the MJO-related CO_2 anomalies in the tropics are well correlated with the lower tropospheric upward velocity. However, such a correlation is not significant at high latitudes. Figure 3b overlays the MJO-related 850 hPa vertical wind (ω_{850hPa}) anomalies on the MJO-related CO_2 anomalies. ω_{850hPa}, defined as the vertical pressure velocity (positive for downward motions), are also obtained from the National Centers for Environmental Prediction/National Center for Atmospheric Research (NCEP/NCAR) Reanalysis (Kalnay et al., 1996). The ω_{850hPa} anomalies are featured with small-scale patches and lack of large-scale structures that the CO_2 anomalies possess. The correlation coefficient between the ω_{850hPa} and CO_2 anomalies over the Arctic region is only −0.04, suggesting that the CO_2 anomalies are not originated from the lower troposphere.

4. Discussions

The MJO is known to be an important source of predictability in the extratropical dynamics and weather on the intraseasonal time scales during the boreal wintertime (Jones et al., 2004; Jung et al., 2010; Kim et al., 2006; Lin, Brunet, & Fontecilla, 2010; Lin, Brunet, & Mo, 2010; Pan & Li, 2008; Vitart & Molteni, 2010). The Arctic CO_2 variability presented in the last section provides another aspect of the teleconnection between the MJO and the polar atmosphere. To unveil the underlying mechanisms that relate the MJO to Arctic CO_2 would require a detailed tracer transport modeling, which is beyond the scope of this work. In the following, a phenomenological study based on correlation analysis will be presented.

A well-known MJO teleconnection pathway is through barotropic vorticity perturbations in the upper troposphere resulting from tropical diabatic heating associated with the convective events, which is manifested as a perturbation in the geopotential height (GPH) near the tropopause (Ferranti et al., 1990; Kiladis et al., 2001; Weare, 2010). As a result, the MJO-related tropopause variations cause observable changes in the lower stratospheric O_3 over the Arctic; such O_3 changes over the MJO cycle are well correlated with the GPH anomalies at 250 hPa (Li et al., 2013; Tian et al., 2007). To examine whether barotropic vorticity perturbations cause the MJO-related Arctic CO_2 anomalies, Figure 3c overlays the MJO-related 500 hPa GPH anomalies on the MJO-related CO_2 anomalies. The GPH data are obtained from NCEP/NCAR Reanalysis. In the GPH anomalies, there are clear signatures of the Pacific-North American pattern extending from the North Pacific to the North America during Phases 8 + 1, 2 + 3, and 4 + 5. The 500 hPa GPH anomalies are similar to the 250 hPa GPH anomalies near the tropopause (Li et al., 2013; Tian et al., 2007). However, the GPH PNA signatures are absent in the CO_2 anomalies. The correlation coefficient between the GPH and CO_2 anomalies over the Arctic region north of 60°N across the MJO phases is only 0.06, suggesting that the CO_2 anomalies are not caused by barotropic vorticity perturbations.

Another consequence of the MJO tropical diabatic heating is the generation of potential vorticity (PV) (Schubert & Masarik, 2006). Zhang and Ling (2012) examined the structure of the MJO-related tropical midtropospheric PV anomalies and concluded that the MJO was not dependent on Kelvin and Rossby waves, in contrast to the suggestions in some studies (e.g., Wang & Rui, 1990; Wedi & Smolarkiewicz, 2010). To date, only the tropical portion of the MJO-related PV anomalies has been studied. For the current work, the MJO-related PV anomalies in the extratropics will be examined.

Assimilated PV available from the ECMWF-Interim Reanalysis (Dee et al., 2011) is used to create a MJO composite. Zhang and Ling (2012) examined the isobaric PV in the tropics to take into account diabatic

processes. For high latitudes, isentropic PV is more appropriate for monitoring tracer movements. The MJO-related PV anomalies at several tropospheric and stratospheric isentropes are compared with the MJO-related CO_2 anomalies in Figure 1 (for the 475 K isentrope) and Figure S1 in supporting information (for the 350 K, 380 K, and the 530 K). In the extratropics, the 350 K and 380 K isentropes are in the midtroposphere (500 hPa) and near the tropopause (250 hPa), respectively, while the 475 K and 530 K isentropes are in the lower stratosphere near the pressure levels 70 hPa and 50 hPa, respectively. The correlation coefficients between the MJO-related anomalies of the isentropic PV and CO_2 over the Arctic (north of 45°N) are listed in Table 1. The correlation is very low (−0.09 at 350 K) in the midtroposphere, and it becomes stronger at the tropopause (−0.21 at 380 K). In the lower ~~troposphere~~ at 475 K, the correlation coefficient between the PV_{475K} and CO_2 anomalies over the Arctic region is −0.44, which, though moderate, is much more significant than the tropospheric quantities examined in previous sections. At 530 K, the spatial pattern of the MJO-related PV_{530K} anomalies is similar to those of PV_{475K}, but the correlation coefficient decreases again to −0.32. Therefore, the PV at 475 K (hereafter denoted by PV_{475K}) has the strongest correlation with the MJO-related CO_2 anomalies. The PV_{475K} anomalies show large-scale structures over the Arctic region, which are roughly negatively correlated with the CO_2 anomalies (Figure 1). A simple regression analysis suggests that CO_2 is decreased by ~0.6 ppm (or 0.2% of the mean CO_2 level) over the Arctic region when PV_{475K} is increased by ~1 potential vorticity unit (or 3% of the mean PV_{475K}).

typo: stratosphere

The finite correlation between the MJO-related CO_2 and PV_{475K} anomalies may seem to be counterintuitive because the AIRS IR channels selected for the CO_2 retrieval have the strongest sensitivity to the troposphere. However, Figure S1 of Chahine et al. (2008) show that, at the polar latitudes, the weighting function of the AIRS CO_2 retrieval has a full width at half maximum covering the pressure range 150–700 hPa. Given that the tropopause is located near 250 hPa over the Arctic, the AIRS CO_2 retrieval represents a column average between the middle troposphere and the lower stratosphere in the Arctic region. Indeed, the weighting function suggests that there is a finite contribution from lower stratosphere between 50 hPa and 250 hPa to the AIRS CO_2 product at polar latitudes.

5. Conclusions

The observation by NASA's AIRS instrument is used to study the impact of MJO on the CO_2 concentration over the Arctic region. The CO_2 concentration north of 60°N varies with a peak-to-peak amplitude of 1.2 ± 0.2 parts per million by volume (ppm) over the MJO cycle. An empirical correlation analysis is applied to diagnose the MJO perturbation with the Arctic CO_2 variability. It is shown that the observed CO_2 anomalies are unlikely to be caused by retrieval bias under cloudy conditions. Instead, the spatial pattern of the MJO-related Arctic CO_2 anomalies resembles that of the isentropic potential vorticity (PV) anomalies at 475 K, with a moderate correlation coefficient −0.44.

Acknowledgments

K. F. L. thanks Ka-Kit Tung and Yuk L. Yung for their advice on the use of the isentropic potential vorticity. K. F. L. also thanks Irene Chen, Sally Newman, Run-Lie Shia, and Xi Xi for reading the manuscript. K. F. L. was supported by NASA grant NNX14AR40G to the University of Washington. The NCEP Reanalysis data are provided by the NOAA/OAR/ESRL PSD, Boulder, Colorado, USA, from their Website at http://www.esrl.noaa.gov/psd/.

References

Aumann, H. H., Chahine, M. T., Gautier, C., Goldberg, M. D., Kalnay, E., McMillin, L. M., … Susskind, J. (2003). AIRS/AMSU/HSB on the aqua mission: Design, science objectives, data products, and processing systems. *IEEE Transactions on Geoscience and Remote Sensing*, *41*(2), 253–264. https://doi.org/10.1109/TGRS.2002.808356

Buchwitz, M., de Beek, R., Burrows, J. P., Bovensmann, H., Warneke, T., Notholt, J., … Schulz, A. (2005). Atmospheric methane and carbon dioxide from SCIAMACHY satellite data: Initial comparison with chemistry and transport models. *Atmospheric Chemistry and Physics*, *5*(4), 941–962. https://doi.org/10.5194/acp-5-941-2005

Chahine, M., Barnet, C., Olsen, E. T., Chen, L., & Maddy, E. (2005). On the determination of atmospheric minor gases by the method of vanishing partial derivatives with application to CO_2. *Geophysical Research Letters*, *32*, L22803. https://doi.org/10.1029/2005GL024165

Chahine, M. T., Chen, L., Dimotakis, P., Jiang, X., Li, Q., Olsen, E. T., … Yung, Y. L. (2008). Satellite remote sounding of mid-tropospheric CO_2. *Geophysical Research Letters*, *35*, L17807. https://doi.org/10.1029/2008GL035022

Ciais, P., Sabine, C., Bala, G., Bopp, L., Brovkin, V., Canadell, J., … Thornton, P. (2013). Carbon and other biogeochemical cycles. In T. F. Stocker, et al. (Eds.), *Climate change 2013: The physical science basis. Contribution of working group I to the fifth assessment report of the intergovernmental panel on climate change* (Chapter 6, pp. 465–570). Cambridge, United Kingdom and New York, NY: Cambridge University Press.

Crevoisier, C., Chedin, A., Matsueda, H., Machida, T., Armante, R., & Scott, N. A. (2009). First year of upper tropospheric integrated content of CO_2 from IASI hyperspectral infrared observations. *Atmospheric Chemistry and Physics*, *9*(14), 4797–4810. https://doi.org/10.5194/acp-9-4797-2009

Dee, D. P., Uppala, S. M., Simmons, A. J., Berrisford, P., Poli, P., Kobayashi, S., … Vitart, F. (2011). The ERA-Interim reanalysis: Configuration and performance of the data assimilation system. *Quarterly Journal of the Royal Meteorological Society*, *137*(656), 553–597. https://doi.org/10.1002/qj.828

Eldering, A., O'Dell, C. W., Wennberg, P. O., Crisp, D., Gunson, M. R., Viatte, C., … Yoshimizu, J. (2017). The orbiting carbon observatory-2: First 18 months of science data products. *Atmospheric Measurement Techniques*, *10*(2), 549–563. https://doi.org/10.5194/amt-10-549-2017

Ferranti, L., Palmer, T. N., Molteni, F., & Klinker, E. (1990). Tropical extratropical interaction associated with the 30-60 day oscillation and its impact on medium and extended range prediction. *Journal of the Atmospheric Sciences*, *47*(18), 2177–2199. https://doi.org/10.1175/1520-0469(1990)047%3C2177:TEIAWT%3E2.0.CO;2

Gruber, N., Keeling, C. D., Bacastow, R. B., Guenther, P. R., Lueker, T. J., Wahlen, M., … Stocker, T. F. (1999). Spatiotemporal patterns of carbon-13 in the global surface oceans and the oceanic Suess effect. *Global Biogeochemical Cycles*, *13*(2), 307–335. https://doi.org/10.1029/1999GB900019

Hashimoto, H., Nemani, R. R., White, M. A., Jolly, W. M., Piper, S. C., Keeling, C. D., … Running, S. W. (2004). El Niño–Southern Oscillation-induced variability in terrestrial carbon cycling. *Journal of Geophysical Research*, *109*, D23110. https://doi.org/10.1029/2004JD004959

Hendon, H. H., & Salby, M. L. (1994). The life-cycle of the Madden-Julian Oscillation. *Journal of the Atmospheric Sciences*, *51*(15), 2225–2237. https://doi.org/10.1175/1520-0469(1994)051%3C2225:TLCOTM%3E2.0.CO;2

Huffman, G. J., Adler, R. F., Bolvin, D. T., Gu, G., Nelkin, E. J., Bowman, K. P., … Wolff, D. B. (2007). The TRMM multisatellite precipitation analysis (TMPA): Quasi-global, multiyear, combined-sensor precipitation estimates at fine scales. *Journal of Hydrometeorology*, *8*(1), 38–55. https://doi.org/10.1175/JHM560.1

Jiang, X., Chahine, M. T., Li, Q., Liang, M.-C., Olsen, E. T., Chen, L. L., … Yung, Y. L. (2012). CO_2 semiannual oscillation in the middle troposphere and at the surface. *Global Biogeochemical Cycles*, *26*, GB3006. https://doi.org/10.1029/2011GB004118

Jiang, X., Chahine, M. T., Olsen, E. T., Chen, L. L., & Yung, Y. L. (2010). Interannual variability of mid-tropospheric CO_2 from atmospheric infrared sounder. *Geophysical Research Letters*, *37*, L13801. https://doi.org/10.1029/2010GL042823

Jiang, X., Wang, J. Q., Olsen, E. T., Pagano, T., Chen, L. L., & Yung, Y. L. (2013). Influence of stratospheric sudden warming on AIRS midtropospheric CO_2. *Journal of the Atmospheric Sciences*, *70*, 2566–2573. https://doi.org/10.1175/Jas-D-13-064.1

Jones, C., Waliser, D. E., Lau, K. M., & Stern, W. (2004). The Madden-Julian Oscillation and its impact on Northern Hemisphere weather predictability. *Monthly Weather Review*, *132*(6), 1462–1471. https://doi.org/10.1175/1520-0493(2004)132%3C1462:TMOAII%3E2.0.CO;2

Jung, T., Miller, M. J., & Palmer, T. N. (2010). Diagnosing the origin of extended-range forecast errors. *Monthly Weather Review*, *138*(6), 2434–2446. https://doi.org/10.1175/2010MWR3255.1

Kalnay, E., Kanamitsu, M., Kistler, R., Collins, W., Deaven, D., Gandin, L., … Joseph, D. (1996). The NCEP/NCAR 40-year reanalysis project. *Bulletin of the American Meteorological Society*, *77*(3), 437–471. https://doi.org/10.1175/1520-0477(1996)077%3C0437:TNYRP%3E2.0.CO;2

Keppel-Aleks, G., Wennberg, P. O., Washenfelder, R. A., Wunch, D., Schneider, T., Toon, G. C., … Wofsy, S. C. (2012). The imprint of surface fluxes and transport on variations in total column carbon dioxide. *Biogeosciences*, *9*(3), 875–891. https://doi.org/10.5194/bg-9-875-2012

Kiladis, G. N., Straub, K. H., Reid, G. C., & Gage, K. S. (2001). Aspects of interannual and intraseasonal variability of the tropopause and lower stratosphere. *Quarterly Journal of the Royal Meteorological Society*, *127*(576), 1961–1983. https://doi.org/10.1002/qj.49712757606

Kim, B. M., Lim, G. H., & Kim, K. Y. (2006). A new look at the midlatitude-MJO teleconnection in the northern hemisphere winter. *Quarterly Journal of the Royal Meteorological Society*, *132*(615), 485–503. https://doi.org/10.1256/qj.04.87

Kuze, A., Suto, H., Nakajima, M., & Hamazaki, T. (2009). Thermal and near infrared sensor for carbon observation Fourier-transform spectrometer on the greenhouse gases observing satellite for greenhouse gases monitoring. *Applied Optics*, *48*(35), 6716–6733. https://doi.org/10.1364/AO.48.006716

Le Quéré, C., Aumont, O., Bopp, L., Bousquet, P., Ciais, P., Francey, R., … Rayner, P. J. (2003). Two decades of ocean CO_2 sink and variability. *Tellus B*, *55*(2), 649–656. https://doi.org/10.1034/j.1600-0889.2003.00043.x

Li, K.-F., Tian, B., Waliser, D. E., & Yung, Y. L. (2010). Tropical mid-tropospheric CO_2 variability driven by the Madden-Julian Oscillation. *Proceedings of the National Academy of Sciences of the United States of America*, *107*(45), 19,171–19,175. https://doi.org/10.1073/pnas.1008222107

Li, K.-F., Tian, B. J., Tung, K.-K., Kuai, L., Worden, J. R., Yung, Y. L., & Slawski, B. L. (2013). A link between tropical intraseasonal variability and Arctic stratospheric ozone. *Journal of Geophysical Research*, *118*, 4280–4289. https://doi.org/10.1002/jgrd.50391

Lin, H., Brunet, G., & Fontecilla, J. S. (2010). Impact of the Madden-Julian Oscillation on the intraseasonal forecast skill of the North Atlantic Oscillation. *Geophysical Research Letters*, *37*, L19803. https://doi.org/10.1029/2010GL044315

Lin, H., Brunet, G., & Mo, R. (2010). Impact of the Madden-Julian Oscillation on wintertime precipitation in Canada. *Monthly Weather Review*, *138*(10), 3822–3839. https://doi.org/10.1175/2010MWR3363.1

Madden, R. A., & Julian, P. R. (1971). Detection of a 40–50 day oscillation in zonal wind in tropical Pacific. *Journal of the Atmospheric Sciences*, *28*(5), 702–708. https://doi.org/10.1175/1520-0469(1971)028%3C0702:DOADOI%3E2.0.CO;2

Madden, R. A., & Julian, P. R. (1972). Description of global-scale circulation cells in tropics with a 40–50 day period. *Journal of the Atmospheric Sciences*, *29*(6), 1109–1123. https://doi.org/10.1175/1520-0469(1972)029%3C1109:DOGSCC%3E2.0.CO;2

Nassar, R., Jones, D. B. A., Kulawik, S. S., Worden, J. R., Bowman, K. W., Andres, R. J., … Worthy, D. E. (2011). Inverse modeling of CO_2 sources and sinks using satellite observations of CO_2 from TES and surface flask measurements. *Atmospheric Chemistry and Physics*, *11*(12), 6029–6047. https://doi.org/10.5194/acp-11-6029-2011

Nevison, C. D., Mahowald, N. M., Doney, S. C., Lima, I. D., Van der Werf, G. R., Randerson, J. T., … McKinley, G. A. (2008). Contribution of ocean, fossil fuel, land biosphere, and biomass burning carbon fluxes to seasonal and interannual variability in atmospheric CO_2. *Journal of Geophysical Research*, *113*, G01010. https://doi.org/10.1029/2007JG000408

Newman, S., Xu, X., Gurney, K. R., Hsu, Y., Li, K.-F., Jiang, X., … Yung, Y. L. (2016). Toward consistency between trends in bottom-up CO_2 emissions and top-down atmospheric measurements in the Los Angeles megacity. *Atmospheric Chemistry and Physics*, *16*(6), 3843–3863. https://doi.org/10.5194/acp-16-3843-2016

Pan, L. L., & Li, T. (2008). Interactions between the tropical ISO and midlatitude low-frequency flow. *Climate Dynamics*, *31*(4), 375–388. https://doi.org/10.1007/s00382-007-0272-7

Rayner, P. J., & O'Brien, D. M. (2001). The utility of remotely sensed CO_2 concentration data in surface source inversions. *Geophysical Research Letters*, *28*, 175–178. https://doi.org/10.1029/2000GL011912

Schubert, W. H., & Masarik, M. T. (2006). Potential vorticity aspects of the MJO. *Dynamics of Atmospheres and Oceans*, *42*(1-4), 127–151. https://doi.org/10.1016/j.dynatmoce.2006.02.003

Susskind, J., Barnet, C. D., & Blaisdell, J. M. (2003). Retrieval of atmospheric and surface parameters from AIRS/AMSU/HSB data in the presence of clouds. *IEEE Transactions on Geoscience and Remote Sensing*, *41*(2), 390–409. https://doi.org/10.1109/TGRS.2002.808236

Tian, B., Yung, Y. L., Waliser, D. E., Tyranowski, T., Kuai, L., Fetzer, E. J., & Irion, F. W. (2007). Intraseasonal variations of the tropical total ozone and their connection to the Madden-Julian Oscillation. *Geophysical Research Letters*, *34*, L08704. https://doi.org/10.1029/2007GL029451

Vitart, F., & Molteni, F. (2010). Simulation of the Madden-Julian Oscillation and its teleconnections in the ECMWF forecast system. *Quarterly Journal of the Royal Meteorological Society*, *136*(649), 842–855. https://doi.org/10.1002/qj.623

Wang, B., & Rui, H. (1990). Dynamics of the coupled moist Kelvin-Rossby wave on an equatorial *b*-plane. *Journal of the Atmospheric Sciences*, *47*(4), 397–413. https://doi.org/10.1175/1520-0469(1990)047%3C0397:DOTCMK%3E2.0.CO;2

Wang, J., Jiang, X., Chahine, M. T., Liang, M.-C., Olsen, E. T., Chen, L. L., … Yung, Y. L. (2011). The influence of tropospheric biennial oscillation on mid-tropospheric CO_2. *Geophysical Research Letters*, *38*, L20805. https://doi.org/10.1029/2011GL049288

Weare, B. C. (2010). Madden-Julian Oscillation in the tropical stratosphere. *Journal of Geophysical Research*, *115*, D17113. https://doi.org/10.1029/2009JD013748

Wedi, N. P., & Smolarkiewicz, P. K. (2010). A nonlinear perspective on the dynamics of the MJO: Idealized large-eddy simulations. *Journal of the Atmospheric Sciences*, *67*(4), 1202–1217. https://doi.org/10.1175/2009JAS3160.1

Wheeler, M. C., & Hendon, H. H. (2004). An all-season real-time multivariate MJO index: Development of an index for monitoring and prediction. *Monthly Weather Review*, *132*(8), 1917–1932. https://doi.org/10.1175/1520-0493(2004)132%3C1917:AARMMI%3E2.0.CO;2

World Meteorological Organization (2016). *Greenhouse gas bulletin no. 12: The state of greenhouse gases in the atmosphere based on global observations through 2015*. Geneva: World Meteorological Organization.

Wong, K. W., Fu, D., Pongetti, T. J., Newman, S., Kort, E. A., Duren, R., … Sander, S. P. (2015). Mapping CH_4:CO_2 ratios in Los Angeles with CLARS-FTS from Mount Wilson, California. *Atmospheric Chemistry and Physics*, *15*(1), 241–252. https://doi.org/10.5194/acp-15-241-2015

Wunch, D., Toon, G. C., Blavier, J. F. L., Washenfelder, R. A., Notholt, J., Connor, B. J., … Wennberg, P. O. (2011). The total carbon column observing network. *Philosophical Transactions of the Royal Society A*, *369*(1943), 2087–2112. https://doi.org/10.1098/rsta.2010.0240

Zhang, C., & Ling, J. (2012). Potential vorticity of the Madden-Julian Oscillation. *Journal of the Atmospheric Sciences*, *69*(1), 65–78. https://doi.org/10.1175/JAS-D-11-081.1

Geophysical Research Letters

Supporting Information for

An intraseasonal variability in CO_2 over the Arctic induced by the Madden-Julian oscillation

King-Fai Li[1,2]
[1] Department of Applied Mathematics, University of Washington, Seattle, WA, USA
[2] Department of Environmental Sciences, University of California, Riverside, CA, USA

Contents of this file
Figure S1

Introduction
In addition to Figure 1 in the text, this supporting information provides a figure showing the correlation between the MJO-related potential vorticity (PV) anomalies and the MJO-related CO_2 anomalies over the Arctic at potential temperature levels (isentropes) 350 K, 380 K, and 530 K.

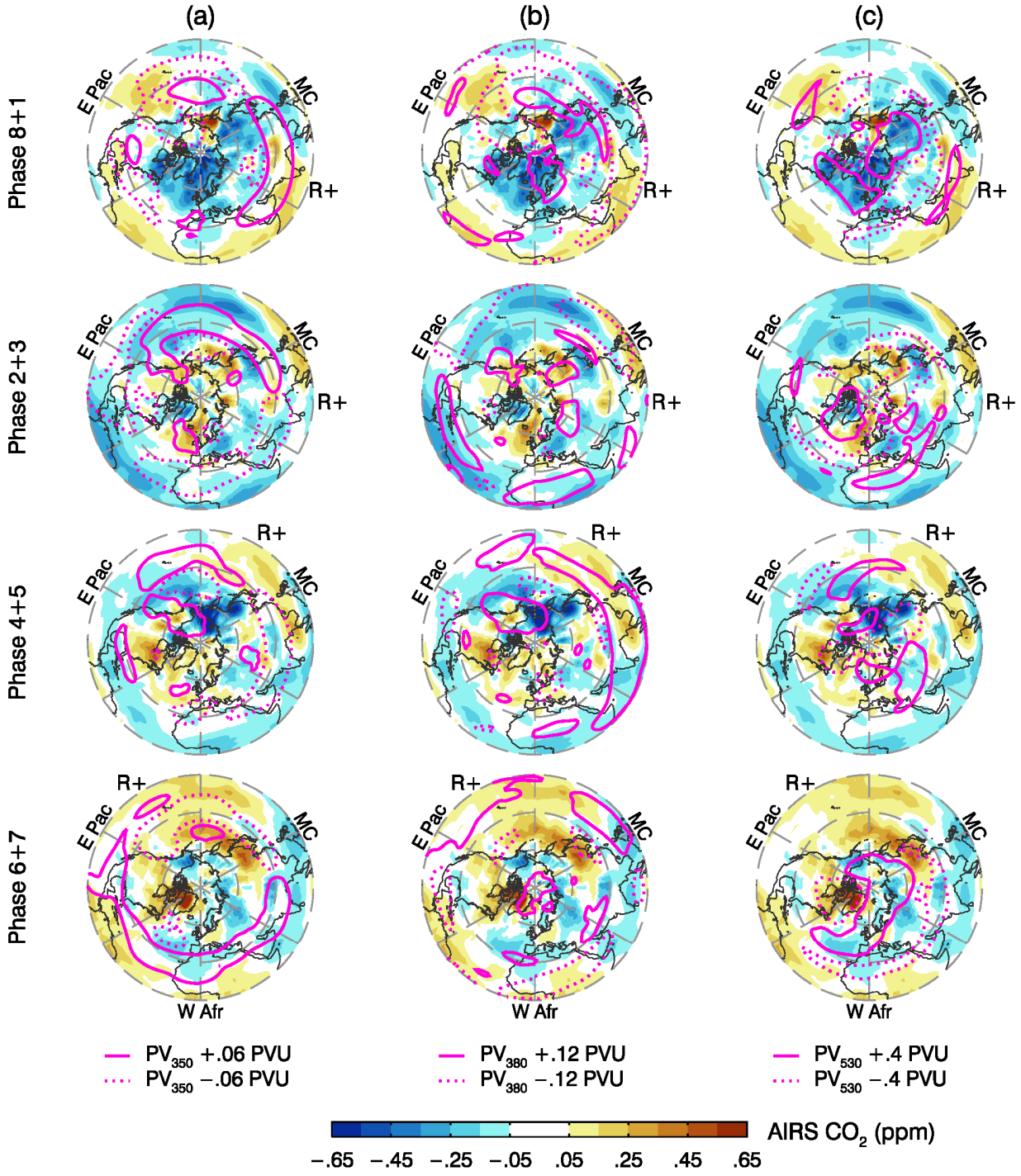

Figure S1. Same as Figure 3 except for correlating the MJO-related CO_2 anomalies (color shades) with PV at isentropes (a) 350 K, (b) 380 K, and (c) 530 K (pink contour lines).